iScience

CellPress
OPEN ACCESS

Article

Single-cell RNA-seq analysis reveals compartment-specific heterogeneity and plasticity of microglia

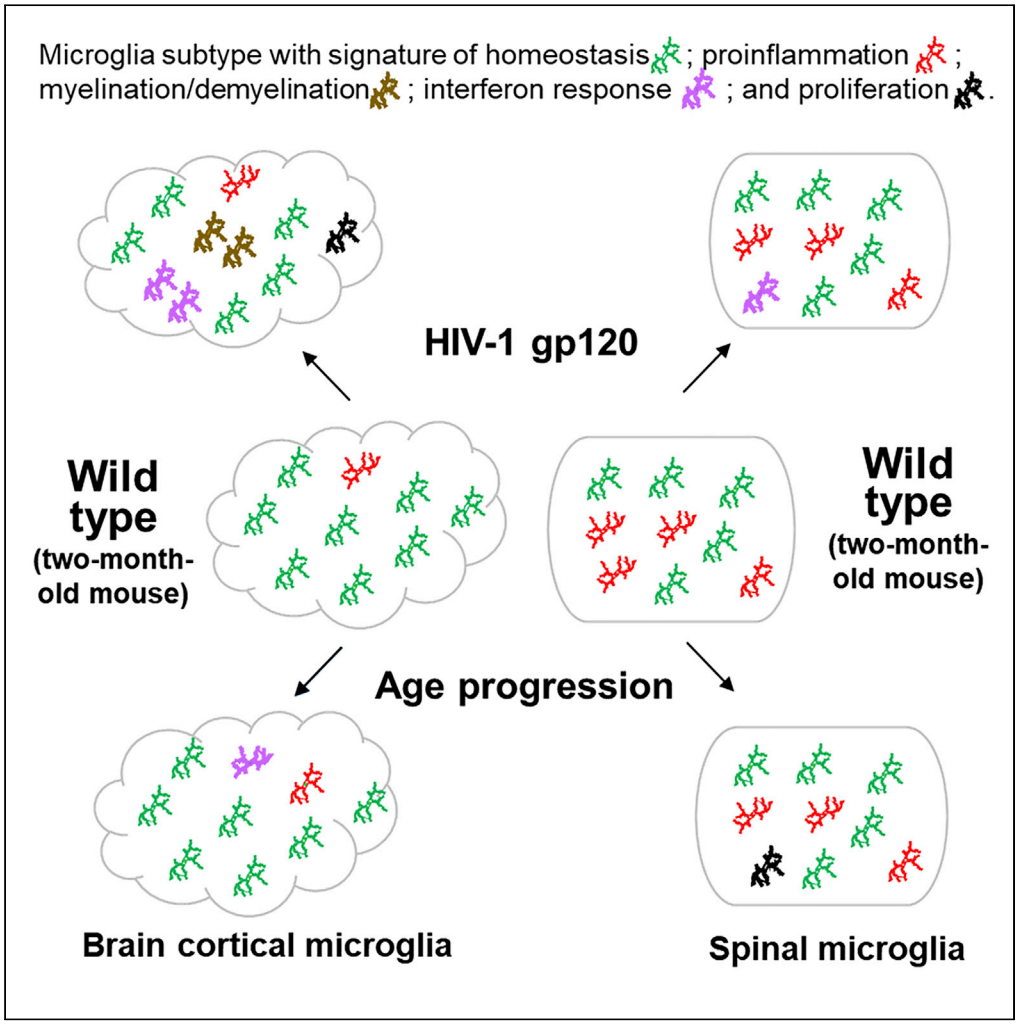

Junying Zheng, Wenjuan Ru, Jay R. Adolacion, ..., Rui Chen, Navin Varadarajan, Shao-Jun Tang

shtang@utmb.edu

HIGHLIGHTS

Mouse cortical and spinal microglia are different in their subtype ratios

Cortical and spinal microglia differentiate differently during age progression

Cortical and spinal microglia differentiate differently in HIV-1 gp120 mice

Zheng et al., iScience *24*, 102186
March 19, 2021
https://doi.org/10.1016/j.isci.2021.102186

iScience

CellPress
OPEN ACCESS

Article

Single-cell RNA-seq analysis reveals compartment-specific heterogeneity and plasticity of microglia

Junying Zheng,[1,7] Wenjuan Ru,[1,7] Jay R. Adolacion,[2,7] Michael S. Spurgat,[1] Xin Liu,[1] Subo Yuan,[1] Rommel X. Liang,[3] Jianli Dong,[3] Andrew S. Potter,[4] S Steven Potter,[4] Ken Chen,[5] Rui Chen,[6] Navin Varadarajan,[2] and Shao-Jun Tang[1,8,*]

SUMMARY

Microglia are ubiquitous central nervous system (CNS)-resident macrophages that maintain homeostasis of neural tissues and protect them from pathogen attacks. Yet, their differentiation in different compartments remains elusive. We performed single-cell RNA-seq to compare microglial subtypes in the cortex and the spinal cord. A multi-way comparative analysis was carried out on samples from C57/BL and HIV gp120 transgenic mice at two, four, and eight months of age. The results revealed overlapping but distinct microglial populations in the cortex and the spinal cord. The differential heterogeneity of microglia in these CNS regions was further suggested by their disparity of plasticity in response to life span progression and HIV-1 pathogenic protein gp120. Our findings indicate that microglia in different CNS compartments are adapted to their local environments to fulfill region-specific biological functions.

INTRODUCTION

The CNS-resident macrophages–microglia play critical roles in CNS development, homeostasis, and inflammation. During development, microglia participate in neural circuit formation by regulating specific processes such as axon outgrowth and synapse maturation and pruning (Hoshiko et al., 2012; Schafer et al., 2013). In adults, microglia actively survey the microenvironment to maintain homeostasis (Brioschi et al., 2019; Liu et al., 2019; Nimmerjahn et al., 2005). In response to infection or injury, microglia are activated to remove pathogens, damaged cells, and dysfunctional synapse and facilitate tissue repair (Gehrmann et al., 1995).

The diverse functionality likely arises from different microglial subtypes with distinct morphologies and biological activities. For instance, activated non-phagocytic microglia appear bushy with short thick branches, undergo rapid proliferation, and secrete pro-inflammatory signaling molecules (Aloisi, 2001), whereas activated phagocytic microglia show an ameboid shape and can travel to injury sites to engulf cell debris (Aloisi, 2001; Brioschi et al., 2019). Activated microglia were used to be classified into pro-inflammatory M1 and anti-inflammatory M2 subtypes. However, emerging evidence suggests that this dichotomous model is insufficient to describe microglial heterogeneity, which likely includes a spectrum of microglial subtypes (Ginhoux et al., 2016; Ransohoff, 2016). The biological basis of microglial heterogeneity is still poorly understood.

Single-cell RNA-seq (scRNA-seq) provides powerful means to characterize microglial heterogeneity. Transcriptomic data generated from this approach revealed novel microglial subtypes (Keren-Shaul et al., 2017; Li et al., 2019). Microglia appear more heterogeneous during early development, compared with adult stages (Li et al., 2019; Masuda et al., 2019). Yet, microglia in adult brains are still plastic and can adapt to different phenotypes in response to pathogenic insults. At least four activated microglial subtypes with hallmarks of inflammation, proliferation, interferon response, and demyelination, respectively, have been identified in mouse models of aging and neurodegenerative diseases (Friedman et al., 2018; Hammond et al., 2019; Keren-Shaul et al., 2017; Li et al., 2019; Masuda et al., 2019; Mathys et al., 2017).

Emerging scRNA-seq evidence suggests spatial and temporal heterogeneity of microglia in the brain (Brioschi et al., 2019). These findings indicate regional and age-dependent plasticity of microglia. However, the

[1]Department of Neuroscience, Cell Biology, & Anatomy, The University of Texas Medical Branch, 301 University Boulevard, Galveston, TX 77555, USA

[2]Department of Chemical & Biomolecular Engineering, University of Houston, Houston, TX 77004, USA

[3]Department of Pathology, The University of Texas Medical Branch, Galveston, TX 77555, USA

[4]Division of Developmental Biology, Children's Hospital Medical Center, Cincinnati, OH 45229, USA

[5]Department of Bioinformatics and Computational Biology, Division of Quantitative Sciences, The University of Texas MD Anderson Cancer Center, Houston 77030, TX, USA

[6]Department of Molecular and Human Genetics, Baylor College of Medicine, Houston 77030, TX, USA

[7]These authors contributed equally

[8]Lead contact

*Correspondence: shtang@utmb.edu

https://doi.org/10.1016/j.isci.2021.102186

mechanism and biological significance of the spatiotemporally regulated microglial heterogeneity are unclear.

In this study, we performed scRNA-seq analysis on 119,833 unsorted cells dissociated from two-, four- and eight-month-old wild type (Wt) and transgenic (Tg) brain cortices and spinal cords. We identified 32,898 microglia and compared microglial heterogeneity in the cortex and the spinal cord of adult mice. We found that, in Wt mice, both cortical and spinal microglia consisted of the homeostatic and inflammatory subtypes although at differential proportions and that cortical and spinal microglia responded differently to age progression. We further demonstrated differential plasticity of microglia in cortices and spinal cords in a mouse model of human immunodeficiency virus (HIV)-associated neurological complications. The findings suggest a region-specific mechanism in controlling the expression of microglial phenotypes and the differentiation of microglial functions in different CNS compartments.

RESULTS

Microglial heterogeneity in the brain cortex and the spinal cord from two-month-old wild-type adult mice

To understand the spatial heterogeneity of microglia in the CNS in an unbiased manner, we performed droplet-based scRNA-seq (Macosko et al., 2015) on cells dissociated from two-month-old Wt adult mouse brain cortices and spinal cords (Figures S1A–S1D). With the intention for an unbiased analysis, we did not perform prior fluorescence-activated cell sorting (FACS). We adapted and optimized a density gradient cell separation protocol (Brewer and Torricelli, 2007) to minimize cell death from dissociation processes and collected the fractions enriched with microglia for the downstream scRNA-seq processing (Figure S1A). Cells dissociated from two cortices and two whole spinal cords were pooled, respectively. A total of 19,960 unsorted cells from the two-month-old cortices (10,000) and spinal cords (9,961) were sequenced to a depth of ~30,000 raw reads per cell. We set the filter criteria of minimal genes = 300 and mitochondrial gene proportion $\leq$10% as a quality control (QC) for scRNA-seq data to remove the dead and the low-quality cells. A total of 5,211 cells from the cortex (52% of cortical cells) and 3,780 cells from the spinal cord (38% of spinal cells) passed quality control for downstream analysis. We performed t-distributed stochastic neighbor embedding (t-SNE) (Seurat, version 2.21) to cluster the cortical and spinal cells. The analyses identified 14 clusters (Figures 1A and S1C), and individual clusters displayed characteristic expression of specific sets of genes (Figure S1D) that defined the cell types of each cluster (Figures 1A and S1C). We found all major types of cells in the clusters of cortical cells, including neurons, microglia, astrocytes, and oligodendrocytes, with neurons markedly underrepresented (Figure 1A). Similar cell types were detected in the spinal clusters, except that few neurons were present (Figure 1B). These data indicate that microglia were the predominant clusters in both the cortical and spinal cells, with few neurons due to the fraction we collected (Figure S1A).

We used the gene markers *Cx3cr1*, *P2ry12*, and *Tmem119* to identify microglia (Figures 1A and 1B). Three microglial clusters were identified from the cortex (Figure 1A) and two microglial clusters from the spinal cord (Figure 1B). These observations indicated a difference between cortical and spinal microglia. To visualize this difference, we performed canonical correlation analysis on pooled cortical and spinal microglia. As shown in Figure 1C, cortical and spinal microglia only partially overlapped, showing differences in the transcriptomic expression of the two microglial populations.

To gain more insights into the biological basis of the differences between cortical and spinal microglia, we sought to determine the microglial subtypes of individual clusters based on their differentially expressed genes. We found that two major clusters in the cortical microglia (clusters 0 and 2 in Figure 1A) showed high expression of homeostatic genes (e.g., *Cx3cr1*, *Tmem119*, *P2ry12*, and *Csf1r*) (Masuda et al., 2019) and thus named them as homeostatic microglia (HOM-M) (Figures 1A and S2A). The HOM-M subtype constituted 96% of cortical microglia. As shown by the clusters on the t-SNE plot (Figure 1A) and gene expression heatmap (Figure 1D), the cortical HOM-M consisted of two computationally polarized groups, HOM-M1 and HOM-M2. HOM-M2 has slightly lower expression of genes coding ribosomal proteins (e.g. *Rps11*, *Rps21*, *Rpl26*) and *Rgs10*, the gene coding a member of regulator of G-protein signaling family (Hunt et al., 1996) (Figures 2A and S3). HOM-M (HOM-M1 and HOM-M2) were enriched with the expression of genes in various molecular pathways that are implicated in maintaining homeostatic functions such as *P2ry12*, consistent with a role of HOM-M in damage sensing (Haynes et al., 2006). We also found HOM-M in the spinal microglia, corresponding to cluster 0 on the spinal t-SNE plot (Figure 1B). The spinal

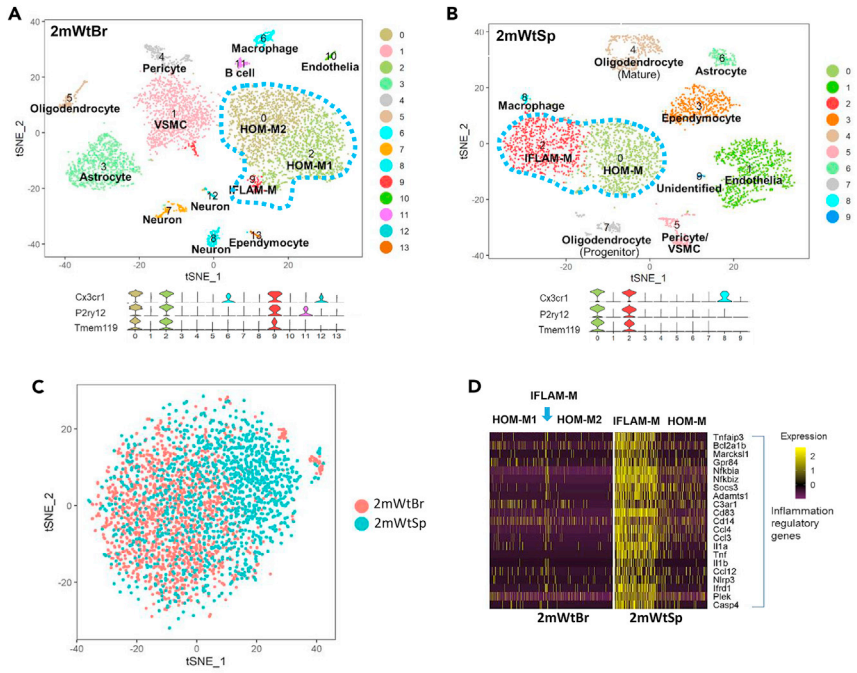

Figure 1. Single-cell RNA-seq (scRNA-seq) analysis revealed region-specific microglial subtypes from the two-month-old wild-type (Wt) brain cortex (2mWtBr) and spinal cord (2mWtSp)

(A and B) t-SNE plots identified microglial clusters (blue dot line circled) in 2mWtBr (A) and 2mWtSp (B). Based on the expressed signature genes, the microglial clusters were defined as homeostatic microglia (HOM-M) and proinflammatory microglia (IFLAM-M). The cortical HOM-M were further segregated into HOM-M1 and HOM-M2 groups. Violin plots below the t-SNE plots show the expression of the microglial markers *Cx3cr1*, *P2ry12*, and *Tmem119* from the t-SNE clusters. We defined the clusters with detectable expression of all three markers as microglia. VSMC: vascular smooth muscle cell.

(C) Seurat's canonical correlation analysis (CCA) showed that spinal microglia partially overlapped with cortical microglia, indicating cortical and spinal specific microglial heterogeneity.

(D) Gene expression heatmap shows the population of inflammatory microglia was big in the spinal cord but small in the cortex. The columns in D represent the subset of all microglia from 2mWtBr and 2mWtSp. Each row: a gene; each column: a microglial cell. See also Figures S1 and S2.

HOM-M constituted 55% of the microglial population. In contrast to the polarization of cortical HOM-M into two groups (HOM-M1 and HOM-M2), the spinal HOM-M were not further polarized within the subtype into different clusters (Figures 1B and 1D).

Another microglial subtype was identified by its unique expression of genes regulating the immune response (e.g. *Il1a*, *Il1b*, *Ccl3*, *Ccl4*) and thus named inflammatory microglia (IFLAM-M). This subtype corresponded to cluster 9 in the cortical t-SNE plot (Figure 1A). Microglia enriched with cytokine and chemokine genes (e.g. *Il1b*, *Ccl2*, *Ccl4*) were previously found from scRNA-seq analysis of human and mouse brains (Hammond et al., 2019; Masuda et al., 2019). They were described as inflammatory microglia (Hammond et al., 2019) or preactivated microglia (Masuda et al., 2019). The IFLAM-M were enriched with the expression of genes involved in cytokines such as *Il1b*, indicating the biological function of this subtype of microglia in mediating proinflammation. Cortical microglia from two-month-old mice only had a small population (4%) of IFLAM-M (Figures 1A, 1D, and S2A). In contrast, IFLAM-M constituted 45% of spinal microglia in two-month-old mice (cluster 2 in Figure 1B; Figures 1D and S2B). The different sizes of cortical and spinal IFLAM-M populations were confirmed by the feature plots of microglial marker genes (*Cx3cr1*, *P2ry12*, *Tmem119*, and *Csf1r*) and IFLAM-M-enriched genes (Figure S2).

The temporal differentiation of cortical and spinal microglial plasticity

The observations of differentiation of cortical but not spinal HOM-M and the drastic difference in population sizes of HOM-M and IFLAM-M in the cortex and the spinal cord suggest differential heterogeneity of

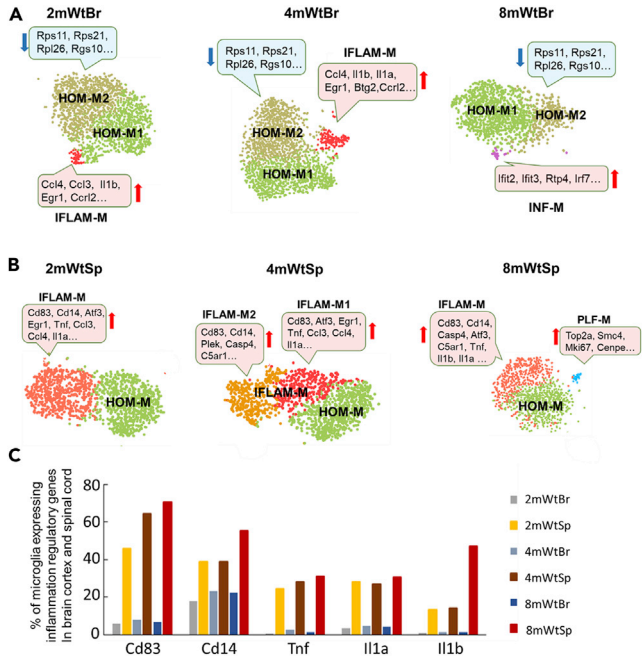

Figure 2. Different temporal plasticity of mouse cortical and spinal microglial heterogeneity

(A) The temporal profiles of cortical microglial subtypes in two-, four-, and eight-month-old Wt mice. HOM-M were polarized into HOM-M1 and HOM-M2 at all ages. HOM-M2 displayed with a characteristic down-regulation of genes including *Rps11*, *Rps21*, *Rpl26*, *Rgs10* (blue boxes) genes coding for ribosomal protein and regulator of G protein signaling. IFLAM-M subtype was a small subtype of cortical microglia identified at two and four months but not at eight months. A subtype of interferon related microglia (INF-M) appeared at 8 months. The highly expressed genes in specific clusters are indicated in pink boxes. We only highlighted genes upregulated (red) or downregulated (blue) in the corresponding clusters compared to HOM-M1.

(B) The temporal profiles of spinal microglial subtypes in two-, four- and eight-month-old Wt mice. IFLAM-M were segregated into two sub-clusters (IFLAM-M1 and IFLAM-M2) at 4 months with their specific set of upregulated genes (pink boxes). At eight months, a small microglial cluster expressing genes regulating cell cycle and proliferation (PLF-M) appeared.

(C) Quantitative differences of cortical and spinal microglia expressing specific inflammation-related genes at different ages. Spinal microglia had a markedly higher portion to express a set of inflammatory regulatory genes than cortical microglia, at all ages checked. See also Figures S3–S5.

cortical and spinal microglia in the two-month-old mice. Next, we sought to determine if the cortical and spinal microglia showed different plasticity. To this end, we compared transcriptomes of cortical and spinal microglia at different animal ages (two, four, and eight months). The remarkable differences in population sizes of HOM-M and IFLAM-M in the cortex and spinal cord revealed at two months of age were also seen at four and eight months (Figures 2A, 2B, and S4). HOM-M were the majority cortical microglia, with 96%, 92%, and 98% at two, four, and eight months, respectively, whereas the cortical IFLAM-M only appeared at two and four months, with 4% and 8%, respectively.

Same as with two-month-old microglia, cortical HOM-M were polarized into HOM-M1 and HOM-M2 at four and eight months (Figure 2A). Compared to HOM-M1, HOM-M2 expressed relatively lower levels of genes coding ribosomal protein and regulator of G-protein signaling (e.g. Rps11, Rps21, Rpl26, Rgs10) (Figure S3). The functional difference between these two clusters is unknown. However, the recent findings of microglial RGS10 as an anti-inflammatory and neuroprotective mediator (Lee et al., 2011) suggest that HOM-M1 and HOM-M2 may play different roles in CNS inflammation and homeostasis maintenance. In contrast to the cortical microglia, no polarization of spinal HOM-M was observed at all ages (Figure 2B).

The cortical IFLAM-M comprised 4% and 8% of total cortical microglia at two and four months, respectively (Figure 2A). These microglia expressed inflammatory cytokines (e.g. Il1b, Ccl3, CCL4). At eight months, the cortical IFLAM-M were not detected. Unlike the small number of cells in the cortical IFLAM-M clusters, the

spinal IFLAM-M comprised a large population (41%–54%) of spinal microglia. Spinal IFLAM-M displayed evident alteration during aging. At two and eight months, they formed one cluster (Figure 2B). While at four months, IFLAM-M were segregated into two clusters, IFLAM-M1 and IFLAM-M2 (Figure 2B). IFLAM-M1 expressed genes (e.g. *Atf3*, *Zfp36*, *Jun*, *Ccl4*, *Ccl3*, *Tnf*, *Il1α*) that regulate acute response and inflammation (McMahon and Monroe, 1996; Sokol and Luster, 2015), while IFLAM-M2 expressed genes (e.g. *Cd14*, *Gpr84*, *C5ar1*, *C3ar1*) that module microglia activation (Bouchard et al., 2007; Janova et al., 2016) and complement response (Freeley et al., 2016). In addition, we found that the percentage of microglia expressing *Cd83*, *Cd14*, and *Il1b* increased in the spinal cord at eight months (Figure 2C) but not in the brain cortex, suggesting a polarization of spinal microglia toward a pro-inflammatory phenotype at this stage (Janova et al., 2016; Rothwell and Luheshi, 2000).

At eight months, a small cortical microglial cluster (2% of cortical microglia) with the signature of interferon response genes (e.g. *Ifit2*, *Ifit3*, and *Ifi204*) emerged (Figures 2A and S5) and was named as interferon response microglia (INF-M). Interferon-related microglia were also found in an Alzheimer disease mouse model (Friedman et al., 2018) and aged mouse brains (Hammond et al., 2019). INF-M and the previously identified interferon-related microglia (Capuccini et al., 2016) shared the expression of multiple interferon-stimulated genes, although fewer members were identified in INF-M. INF-M were not detected in spinal microglia at the same age (Figure 2B).

A small (3%) spinal specific microglial cluster appeared at eight months, with a signature expression of a set of genes implicated in proliferation and cell cycle control (e.g. *Mki67*, *Top2a*) (Figure 2B). We named this cluster as proliferation-related microglia (PLF-M). Microglia expressing proliferative genes were identified in the developing white matter as proliferative-region-associated microglia (PAM) (Li et al., 2019). However, we did not detect in PLF-M the expression of phagocytosis-related genes, which was a signature of PAM (Li et al., 2019). PLF-M were not detected in the cortical microglia. The emerging of PLF-M in the eight-month-old spinal cord suggests a spinal specific microglial proliferation during this age.

Cortical and spinal microglial heterogeneity in HIV-1 gp120 transgenic mice at two months of age

The results described above revealed microglial cortical and spinal specific heterogeneity, and the significance of this compartment-specific heterogeneity is suggested by its age-related differential plasticity. Because microglia are CNS-resident immune cells, we sought to further confirm the biological relevance of the compartment-specific microglial heterogeneity by determining their response to pathogenic challenges. To this end, we used the HIV-1 gp120 Tg mouse, which expresses secreted gp120 in astrocytes. This is a model of HIV-associated neurological disorders and develops various neuropathologies (Toggas et al., 1994). Because evident microglial activation was observed in the CNS, the gp120 Tg mouse would provide a good model to investigate microglial heterogeneity induced by pathogenic agents.

We found that microglial heterogeneity was increased both in the cortex and the spinal cord of the Tg mice at two months of age (Figures 3A and 3B), compared with the age-matched Wt animals (Figures 1A and 1B). Five microglial clusters were identified in the two-month-old Tg cortex (Figure 3A). Based on the transcriptomic signature, these clusters included the HOM-M (cluster 0 and 1), IFLAM-M (cluster 3), INF-M (cluster 8), and PLF-M (cluster 7) (Figure 3A). Compared with that in age-matched Wt mice, two new subtypes PLF-M and INF-M were induced in the transgenic mice (Figures 3A–3D), with each constituting ~4% of total cortical microglia.

Compared with cortical microglia, spinal microglia responded differently in the Tg mice at two months. Three spinal microglial subtypes were identified (Figure 3B) including the HOM-M (cluster 1 and 2), IFLAM-M (cluster 0), and INF-M (cluster 12) (Figures 3B and 3C). While the INF-M subtype, which was not detected in Wt cortical and spinal microglia at two months (Figures 1A and 1B), was induced in both cortical and spinal microglial populations in the Tg mice at the same stage (Figure 3D), the PLF-M subtype was only induced in the Tg cortical microglia but not in the spinal counterpart (Figure 3D).

Age-gp120 interaction differentially promoted cortical and spinal microglial heterogeneity

The data described above revealed differential plasticity of cortical and spinal microglial heterogeneity in response to age progression or gp120-induced pathogenesis. Next, we sought to test the interactive effect of age progression and gp120 on the expression of heterogeneity plasticity of cortical and spinal microglia.

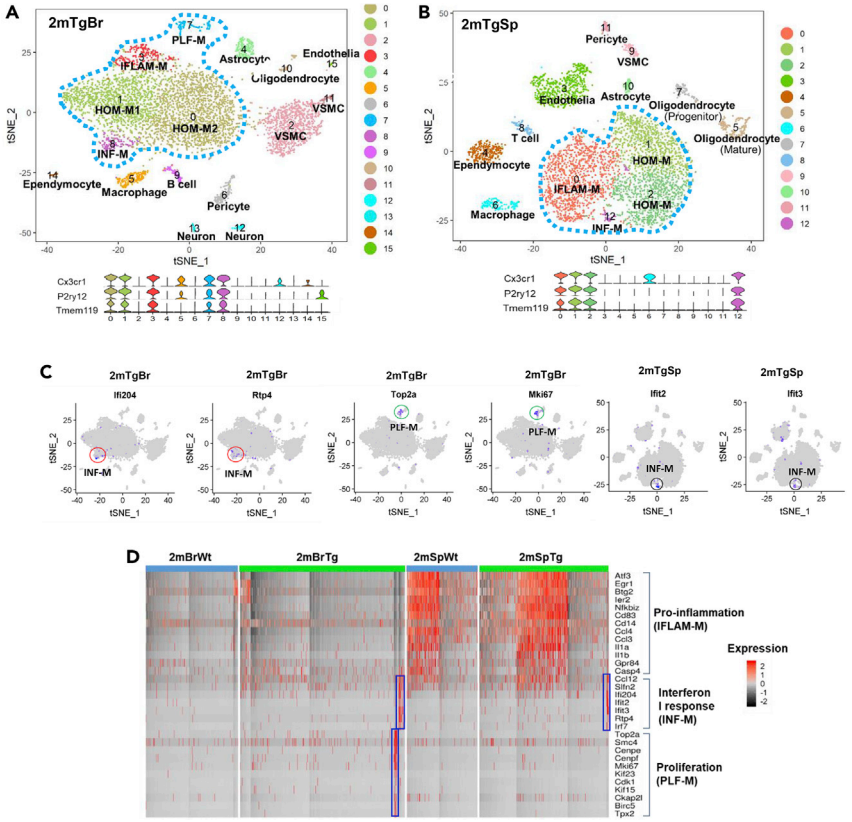

Figure 3. Region-specific microglial heterogeneity in two-month-old HIV-1 gp120 transgenic (Tg) mice

(A and B) t-SNE analysis identified five cortical (2mTgBr) and four spinal (2mTgSp) microglial clusters (circled by blue-dot lines) from the two-month-old Tg mice. The microglial identity was defined by the co-expression of multiple microglial markers as shown in violin plots below t-SNE plots.

(C) Feature plots of signature genes of INF-M (red circles) and PLF-M (green circles) in 2mTgBr and INF-M (black circles) in 2mTgSp demonstrate the portion of the corresponding subtypes in the cortical and spinal microglia.

(D) Heatmap showed both INF-M and PLF-M microglia in the cortex but only INF-M in the spinal cord of the gp120 Tg mice. Gp120 did not significantly change the population of IFLAM-M in the cortex and spinal cord at two months. However, we can see the proportion of spinal IFLAM-M is much larger in both Wt and Tg mice than in the Wt and Tg cortices, respectively. The columns represent the subsets of all microglia from two-month-old Wt and Tg cortices and spinal cords.

To this end, we determined the temporal profiles of cortical and spinal microglial subtypes at different ages (at two, four, and eight months) of the Tg mice. We observed that cortical microglia displayed distinct but overlapping subtypes with age progression. Cortical microglial heterogeneity increased for the two-, four-, and eight-month-old Tg mice, compared with the cortical microglial subtypes from the age-matched Wt mice (Figure 4A). Five cortical microglial subtypes were identified in four-month-old Tg mice: HOM-M (including HOM-M1 and HOM-M2), IFLAM-M, INF-M, and PLF-M, which were detected in the cortical microglia of two-month-old Tg mice, and a fifth new subtype (Figures 4A and 4B). This new subtype comprised 11% of the total cortical microglia and was named as myelination/demyelination-related microglia (MYE-M) because it had the signature expression of genes that promote demyelination and remyelination (e.g. *Lpl*, *Cst7*, *Igf1*, *Spp1*, *Fabp5*, *Itgax*) (Bruce et al., 2018; Ma et al., 2011; Nomura et al., 2017). Compared to the age-matched Wt, the population of IFLAM-M increased in the two- and four-month-old Tg cortices (Figures 4B and 9). The eight-month-old Tg cortical microglia contained similar clusters with the two- and four-month-old Tg cortices except the MYE-M (Figures 4A and 4B). MYE-M that appeared in the four-month-old cortex were not detected in the eight-month-old Tg cortex (Figures 4A and 4B). In contrast, the INF-M and PLF-M remained (Figure 4B). The proportion of INF-M in the cortical microglia gradually increased from two to eight months in the Tg cortices and reached the highest at eight months,

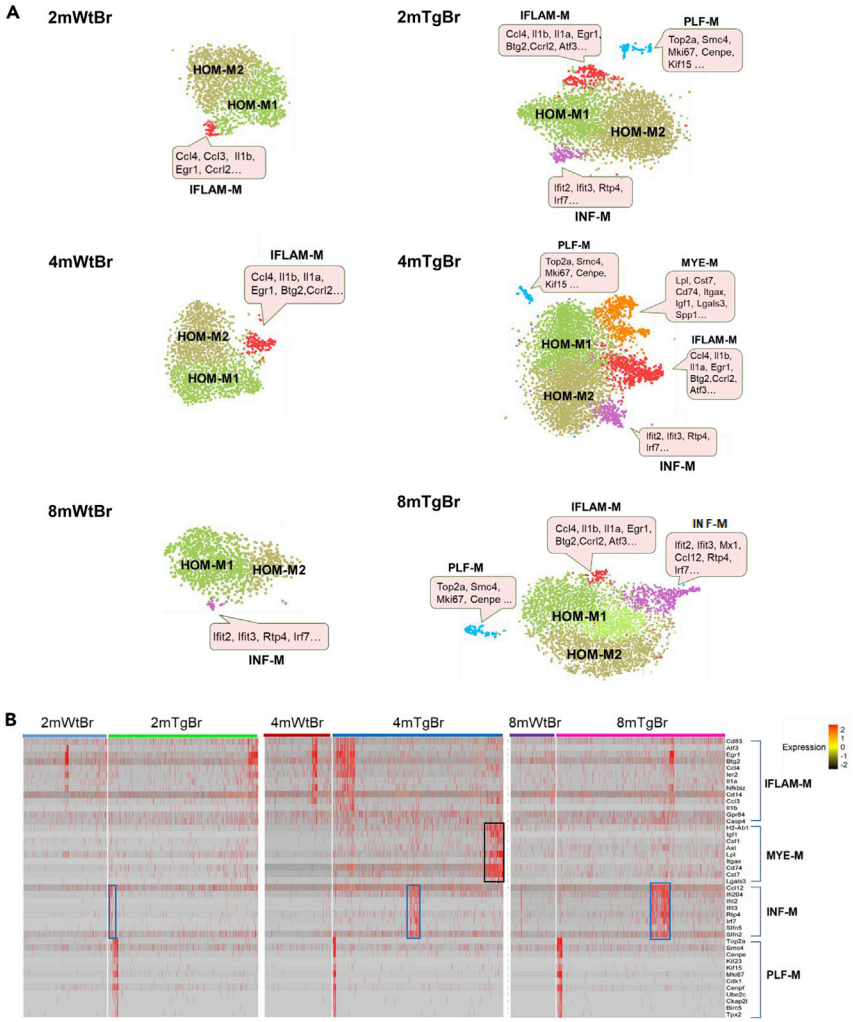

Figure 4. Comparison of the temporal profiles of cortical microglial heterogeneity of Wt and gp120 Tg mice

(A) tSNE plots of Wt and Tg cortical microglia at different ages. The cortical microglial subtypes of the Tg mice at two, four, and eight months increased, compared to the Wt counterparts at the corresponding ages; this was particularly clear at 4 months. The signature genes expressed in the individual clusters were indicated in the pink boxes.

(B) Heatmap showed the expression of feature genes of IFLAM-M, myelination/demyelination-related microglia (MYE-M), INF-M, and PLF-M subtypes. MYE-M (black rectangle) were only observed in the four-month-old Tg cortices, while INF-M (blue rectangle) gradually increased with age progression in Tg cortices. The columns represent the subsets of all microglia from each data set.

covering 11% of the total cortical microglial population (Figures 4B and 9). The population of PLF-M did not show changes in the Tg cortices with age progression (Figures 4B and 9).

We found that MYE-M emerged in the four-month-old cortice particularly interesting as this type of microglia uniquely expressed a set of genes (e.g. *Lpl*, *Cst7*, *Igf1*, *Itgax*, *Lgals3*, *Spp1*) (Figure 5A), which were also the signature genes of the disease-associated microglia (DAM) identified from the brain of Alzheimer disease (Keren-Shaul et al., 2017). However, when comparing the upregulated genes in MYE-M (Table S1 sheet 4mTgBr_cluster_3_MYE-M) with those in DAM, we found that only 13% of the up-regulated genes in MYE-M were expressed in DAM (Figure 5B). This observation suggests that MYE-M and DAM are related but distinct microglial subtypes induced in the HIV-1 gp120 Tg and the Alzheimer disease models, respectively. To verify MYE-M *in vivo*, we performed RNAscope *in situ* hybridization (ISH) of *Cst7* mRNA, in combination with Iba1 immunostaining. The results showed Cst7 mRNA in clusters of microglia in the four-month-old Tg cortex (Figure 5C). $Cst7^{+}$ $Iba1^{+}$ microglia consisted of <1% of total cortical microglia

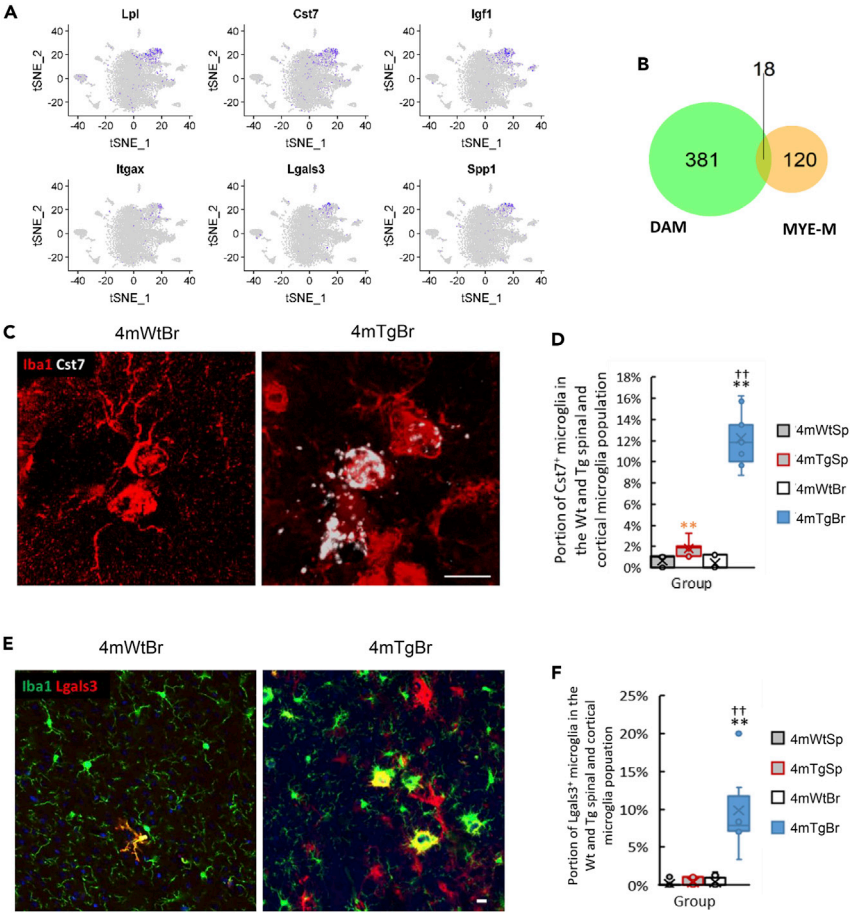

Figure 5. Verification of MYE-M in the Wt and Tg spinal and cortical tissue of four-month-old mice

(A) Feature plots showing the signature genes of MYE-M in the four-month-old Tg cortex (4mTgBr).

(B) Venn diagram showed that 13% of the up-regulated genes in MYE-M were expressed in DAM (disease-associated microglia) identified in Alzheimer disease (see also Table S1).

(C) RNAscope *in situ* hybridization (ISH) demonstrated the expression of *Cst7* mRNAs (white) in the Wt and Tg cortical microglia (red) (labeled by Iba1 immunostaining).

(D) Population of *Cst7*$^{+}$Iba1^{+} microglia in the Wt and Tg cortex and spinal cord.

(E) Fluorescent immunostaining revealed the expression of Lgals3 (red) protein in the Wt and Tg cortical microglia (green) (labeled by Iba1 immunostaining).

(F) The population of Lgals3^{+}Iba1^{+} microglia in the Wt and Tg spinal cord and cortex. **(orange): p value<0.01 4mWtSp vs 4mTgSp. **: p value <0.01 4mWtBr vs 4mTgBr. ††: $p < 0.05$ 4mTgSp vs 4mTgBr. n = 3. Scale bar: 10 μm. Data are represented as mean ± standard error of the mean (SEM).

See also Videos S1 and S2.

in the Wt but increased to 12% in the Tg mice (Figure 5D). We also performed immunostaining of Lgals3, another MYE-M marker. Lgals3^{+} Iba1^{+} microglia in the four-month-old Wt cortex only consisted of 1–2% of total cortical microglia, while Lgals3^{+} Iba1^{+} microglia made up ~10% of the cortical microglia in the four-month-old Tg mice (Figures 5E and 5F), consistent with the finding of 11% MYE-M revealed by scRNA-seq analysis. In contrast to the cortex, both Cst7^{+} Iba1^{+} and Lgals3^{+} Iba1^{+} microglia were very low in the four-month-old Wt and Tg spinal cord (Figures 5D and 5F).

In contrast to the differentiation of multiple new cortical microglial subtypes in the Tg mice at two, four, and eight months compared with the Wt cortical microglia as described above, the spinal microglia in the Tg mice showed fewer new subtypes compared with their age-matched Wt counterparts. We only observed the increase of microglial heterogeneity in the two- and four-month-old Tg mice, with the appearance of INF-M (Figures 6A and 6B) that constituted ~2% of the total spinal microglia population. We performed ISH of *Irf7* mRNA (one of INF-M feature genes revealed by scRNA-seq) to visualize the

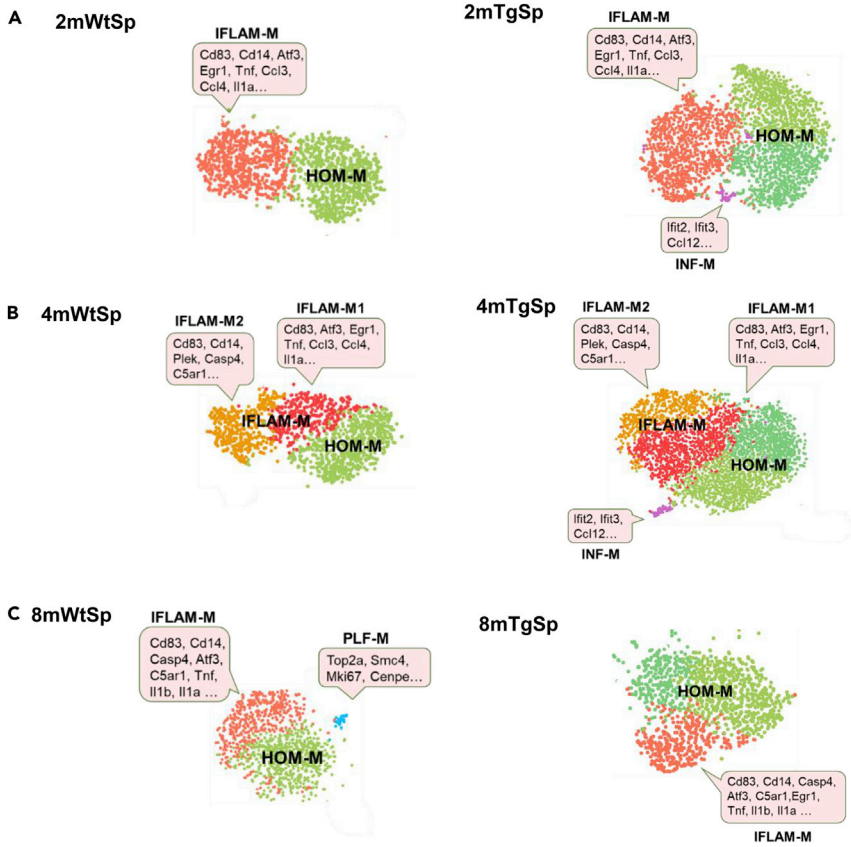

Figure 6. Comparison of the temporal profiles of spinal microglial heterogeneity of Wt and gp120 Tg mice

Compared to their Wt counterparts, INF-M subtype was the only new subtype induced in two- (A) and four-month-old Tg mice (B). On the other hand, the PLF-M subtype detected in Wt mice at eight months was not detected in the Tg mice at this age (C). The signature genes of specific clusters are indicated in pink boxes.

gp120-induced INF-M subtype of microglia in tissues, with Iba1 immunostaining to label microglia (Figure 7A). INF-M in the spinal and cortical tissues of the four-month-old Wt and Tg mice revealed by ISH were quantified (Figure 7B). The INF-M subtype was not detected in the 4-month-old Wt spinal cord but constituted ~1% of the total spinal microglia population in the Tg mice. In the cortex, the INF-M subtype constituted <1% in the Wt but ~5% in the Tg mice. These data were consistent with the scRNA-seq results (Figure 9).

The INF-M subtype was not detected in the eight-month-old Tg spinal cord of either Wt or Tg mice (Figure 6C). In addition, the PLF-M subtype observed in the Wt spinal cord at eight months was not detected in the eight-month-old Tg spinal cord (Figure 6C). Similar to the four-month-old Wt spinal microglia, the IFLAM-M in four-month-old Tg spinal microglia also differentiated into IFLAM-M1 and IFLAM-M2 groups (Figure 6B).

Morphological comparison of HOM-M, MYE-M, and INF-M

After fluorescence staining of Lgals3 (a specific marker for MYE-M), we performed confocal imaging of the 3-D morphologies of MYE-M (Video S1) in four-month-old Tg cortex and compared them with the morphologies of HOM-M (Video S2) in four-month-old Wt cortex. HOM-M had small round-shaped cell bodies with long processes, while MYE-M showed bigger irregular cell bodies with bushy short processes. In contrast to HOM-M that tended to spread, MYE-M often formed clusters, in which cell bodies were in touch with each other and/or their processes were intermingled. Due to the lack of specific antibody, we visualized the morphology of INF-M by combined ISH of *Irf7* mRNA and immunostaining of Iba1 (Video S3). However, less preserved 3-D morphologies of INF-M were imaged due to the thin section (10 μm) and proteinase digestion required for ISH.

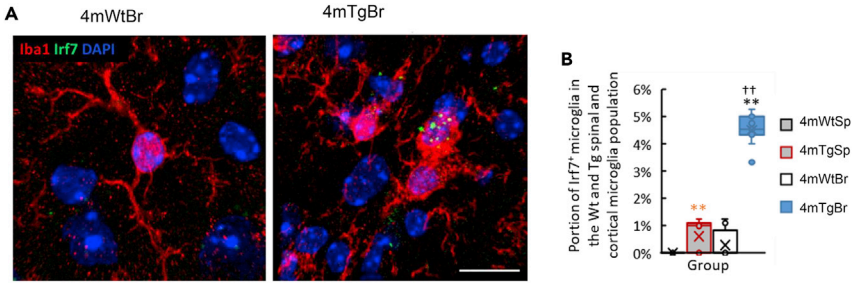

Figure 7. Verification of INF-M in the Wt and Tg spinal and cortical tissue of four-month-old mice

(A) ISH demonstrated the expression of Irf7mRNA (green) (one of INF-M marker genes) in the cortical microglia (red) (labeled by Iba1 immunostaining).

(B) Population of *Irf7*$^{+}$Iba1^{+} microglia in the Wt and Tg spinal cord and cortical tissue of four-month-old. Scale bar: 10 μm. **(orange): p value<0.01 4mWtSp vs 4mTgSp. **: p value <0.01 4mWtBr vs 4mTgBr. ††: p < 0.05 4mTgSp vs 4mTgBr. n = 3. Scale bar: 10 μm. Data are represented as mean ± standard error of the mean (SEM).

Differential biological activity of cortical and spinal microglial subtypes in the gp120 transgenic mice

The above data revealed the differential plasticity of cortical and spinal microglial heterogeneity in the HIV-1 gp120 Tg mouse. We next sought to investigate if the biological functions of the same microglial subtype in the cortex and the spinal cord were differentiated in the cortex and the spinal cord of the Tg mice. To this end, we sought to compare the activity of the canonical pathways of cortical and spinal microglial subtypes in the Wt and gp120 Tg mice. Lists of upregulated genes with the adjusted p value (<0.05) for individual microglial clusters (Tables S1 and S2) from two-, four-, and eight-month-old Wt and Tg cortices and spinal cords were entered into Ingenuity Pathways Analysis to evaluate the change in individual biological pathways (e.g. immune response and nervous signaling pathways). We found that many canonical pathways present in the same subtype of the cortical and spinal microglia were differentially regulated in the Tg mice (Figures 8A–8D). For instance, some selected canonical pathways were evidently activated in both cortical and spinal HOM-M subtypes in Wt mice, especially at two and four months (Figures 8A and 8C). However, these pathways, except the neuroinflammation signaling, were severely attenuated in the cortical HOM-M of the transgenic mice across all ages (Figure 8B). In the spinal cords, however, the attenuation of these pathways seemed to occur but to a lesser degree compared with their cortical counterparts (Figure 8D).

DISCUSSION

In this study, we compared 32,898 microglia from the two-, four-, and eight-month-old cortices and spinal cords using scRNA-seq approaches and characterized microglial subtypes in these CNS compartments based on cluster analysis. Notwithstanding the intrinsic technical caveats associated with scRNA-seq, the multi-way comparisons enabled by including samples from different tissues (cortices and spinal cords), different ages (two, four, and eight months), and different mouse lines (Wt and gp120 Tg) allowed us to evaluate the consistency among the data sets. In addition, our immunofluorescence staining and ISH confirmed the identified microglial subtypes such as MYE-M and INF-M *in vivo*. Our results revealed overlapping but distinct microglial populations in the cortex and the spinal cord (Figure 9). The differential heterogeneity was further shown by the differences in their plasticity under two neurophysiological conditions relevant to the biological function of microglia: life span progression and pathogen exposure. The findings indicated that microglia in the cortical and spinal compartments are adapted to their local environments to fulfill their unique biological functions, by either differentiating into distinct subtypes or expressing differential plasticity of the same subtypes or both.

Cortical and spinal spatiotemporal microglial heterogeneity

We found that microglia in the cortex and the spinal cord in two- and four-month-old Wt mice consisted of two subtypes: HOM-M and IFLAM-M. However, the proportions between HOM-M and IFLAM-M were dramatically different in the cortex and the spinal cord. IFLAM-M comprised only a small portion (4–8%) of the cortical microglia, while about half of microglia were IFLAM-M in the spinal cord (Figure 9). Because IFLAM-M express inflammatory genes and likely play a critical role in the inflammatory response, these observations indicated that the

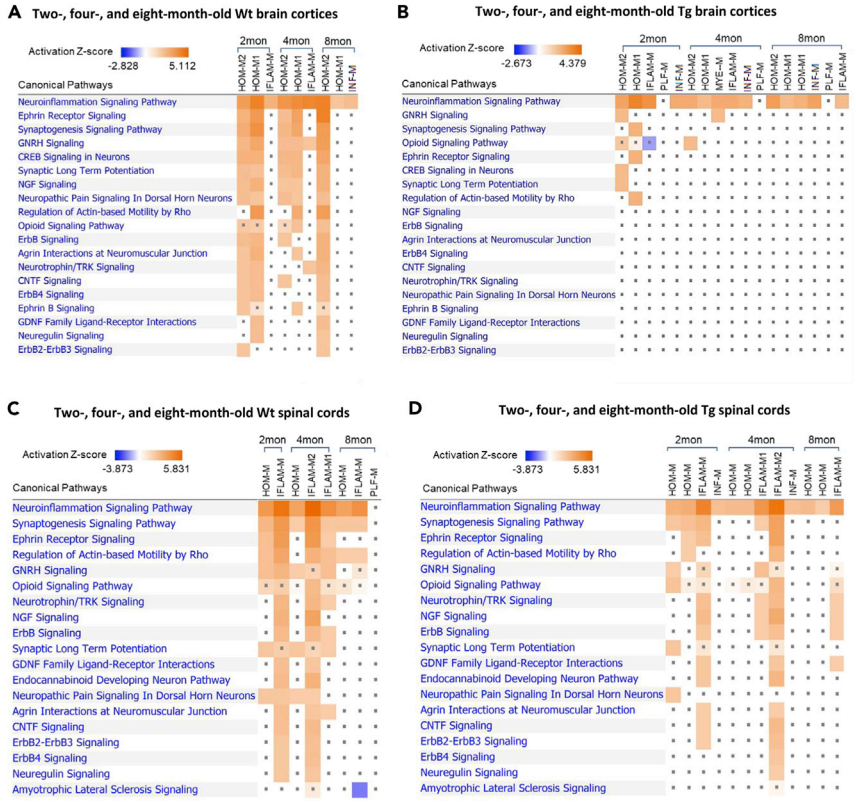

Figure 8. The effect of HIV-1 gp120 on cortical and spinal microglial nervous signaling pathways

(A) Importing the upregulated list of genes of each cluster into Ingenuity Pathway Analysis (IPA) predicted the activated nervous signaling pathways of cortical microglia in the two-, four-, and eight-month-old Wt cortices.

(B) The activated cortical microglial signaling was severely suppressed by gp120 in the Tg brain cortices at all ages.

(C) IPA predicted the activated nervous signaling pathways of spinal microglia in the two-, four-, and eight-month-old Wt spinal cords. (D) The activated nervous signaling of spinal microglia was differentially attenuated by gp120 in the Tg spinal cords. Note the signaling of spinal microglia was attenuated in a less degree compared to that of the cortical microglia. Orange: activated signaling. Blue: inhibited signaling. Dot: not significantly changed.

See also Tables S1 and S2.

cortex may have a more limited capacity in a microglia-mediated inflammatory response. In contrast, the large and more active population of the spinal IFLAM-M suggested an increased capacity for microglia-mediated inflammatory response in the spinal cord. The plasticity of spinal microglia was also suggested by the observation the spinal-specific plastic changes of the IFLAM-M during age progression.

From two months to eight months of age, we did not see drastic changes of HOM-M in both the cortex and the spinal cord in Wt mice. In contrast, spinal IFLAM-M were detected as one cluster at two months, then differentiated into IFLAM-M1 and IFLAM-2 at four months, and returned to one cluster at eight months (Figure 2B). IFLAM-M1 expressed cytokine genes (e.g. *Tnf*, *Il1a*, *Il1b*), and IFLAM-M2 expressed genes regulating cell activation and complementary response (e.g. Cd14, C5ar1, C3ar1).

In the Wt cortex, the IFLAM-M subset disappeared at eight months (Figure 9). And a small new cluster of INF-M was identified at this age. INF-M were characterized by interferon response genes, which are implicated in the age-related modulation of cognitive function (Baruch et al., 2014). Given the observation of aging-induced interferon-related microglia (Friedman et al., 2018; Hammond et al., 2019), the presence of INF-M at eight months may suggest interferon-related microglial activation during aging. It is unclear if there is a causal relationship between the disappearance of IFLAM-M and the appearance of INF-M in the eight-month-old cortex.

In the eight-month-old Wt spinal cord, INF-M were not observed (Figure 9). Instead, a small cluster of PLF-M appeared, constituting 3% of spinal microglia (Figure 9). Because PLF-M expressed genes regulating cell

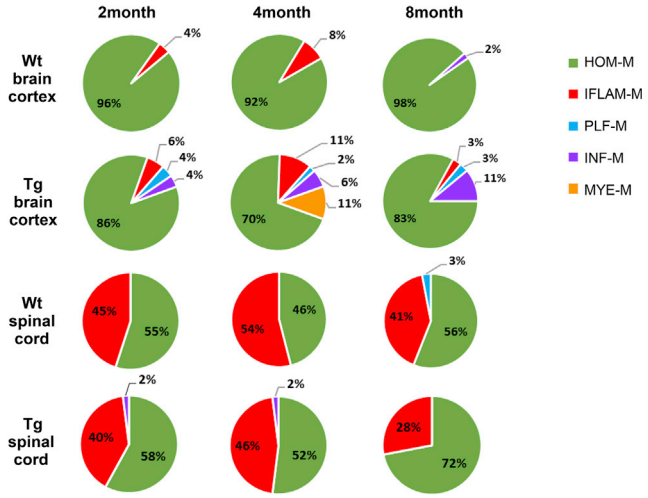

Figure 9. A summary pie chart shows the relative proportions of individual microglial subtypes in Wt and Tg cortices and spinal cords at two, four, and eight months

cycle and proliferation and were not observed in the cortex of Wt mice at this stage, the appearance of spinal PLF-M indicated the occurrence of spinal specific microglial proliferation during this age.

Together, the temporal comparisons of the scRNA-seq analysis of cortical and spinal microglia of Wt mice revealed that microglia in these two CNS compartments have distinct heterogeneity and age-related plasticity. These findings suggest compartment-specific differentiation of the biological function of microglia to maintain local homeostatic function of the CNS.

Cortical and spinal spatiotemporal plasticity of microglial heterogeneity in the HIV-1 gp120 transgenic mice

Temporal comparisons of scRNA-seq analyses revealed marked differences of microglial heterogeneity in the cortex and the spinal cord of the gp120 Tg mice (Figure 9). Relative to their Wt counterparts, in addition to the HOM-M and IFLAM-M subtypes, cortical microglia in the Tg mice formed three new subtypes, i.e., INF-M, MYE-M, and PLF-M, while spinal microglia from transgenic mice only differentiated one new subtype, INF-M (Figure 9). PLF-M and MYE-M were cortical specific in the Tg mice.

Although INF-M subtype was shared by both the Tg cortical and the spinal microglia, it showed different temporal profiles in these compartments. Cortical INF-M were present at all three time points and increased in its proportions with age progression (Figure 9). On the other hand, spinal INF-M appeared at both two and four months with a small, steady percentage but disappeared at eight months (Figure 9). As type I interferon-induced reactive microglia were implicated in engulfing neuronal and synaptic elements (Bialas et al., 2017), the increase of the cortical INF-M population as age progresses may be related to neuronal damages during aging of patients with HIV-1. Type I interferon in the spinal cords is implicated in pain suppression (Liu et al., 2016). It would be of interest in future studies to determine if INF-M subtype contributes to the pathogenesis in the spinal pain neural circuits induced by HIV-1 neurotoxins.

PLF-M subtype was a cortical specific microglial subtype that was present at all stages in the Tg mice but absent in the spinal cord. The presence of PLF-M indicated that this subset of cortical microglia was in proliferating states in the Tg mice. Since cluster of PLF-M is isolated from all other microglial clusters on the tSNE plots, this type of microglia maybe differentiated from a different lineage such as microglia-progenitor cells which would eventually develop into one of the microglial subtypes in the Tg cortex. In contrast, the lack of PLF-M in the spinal cord suggested low proliferation and less diversity of spinal microglia in the transgenic HIV model.

MYE-M subtype was another cortical specific subtype identified in the Tg mice. However, unlike the PLF-M subtype, MYE-M subtype was only detected in the four-month-old Tg cortex (Figure 9). Signature genes of MYE-M (e.g. *Lpl*, *Cst7*, *Igf1*, *Itgax*, *Lgals3*, *Spp1*) (Figure 5A) were also found to be expressed in microglial

subtypes (e.g. DAM) in neurodegeneration models (Friedman et al., 2018; Hammond et al., 2019; Keren-Shaul et al., 2017; Masuda et al., 2019). We compared the upregulated genes from MYE-M and DAM and found only 18 out of 138 MYE-M-enriched genes overlapped with those from DAM (Figure 5B). The overlapping genes included *Cst7*, *Lpl*, and *Itgax* that are involved in myelinogenic processes (Wlodarczyk et al., 2017) and phagocytosis (Reichert and Rotshenker, 2019), suggesting MYE-M might be involved in phagocytosis and myelination. Gp120 induced MYE-M in the Tg brain cortices (Figures 5C and 5E). As DAM was implicated in clearance of damaged neurons associated with Alzheimer disease (Keren-Shaul et al., 2017), it is tempting to speculate a similar role of MYE-M. However, because MYE-M and DAM have many non-overlapping signature genes, these subtypes likely have their specific biological functions. As most MYE-M were observed as clusters, it is possible that they are at a state of proliferation.

Tg expression of gp120 causes synapse loss and glial reaction resembling the abnormalities in brains of patients with HIV (Toggas et al., 1994). Gp120 also induces spinal neuropathologies, including synapse degeneration (Ru et al., 2019; Yuan et al., 2014), myelin abnormalities (Shi. et al., 2016), and microglial activation (Yuan et al., 2014). It would be important for future studies to determine the potential contribution of the gp120-induced microglial subtypes identified in this study to the development of the neurological pathologies.

In summary, our findings reveal differential microglial heterogeneity in the cortex and the spinal cord of mice. They also show that microglia in these two CNS compartments have different plasticity in response to age progression or HIV-1 gp120. The results are consistent with the emerging view that brain and spinal microglia differ in their development (Xuan et al., 2019). It will be interesting for future studies to elucidate the biological function and the differentiation mechanisms of the compartment-associated microglial heterogeneity and plasticity. In addition, given the recent finding of sexual dimorphism of microglia (Bordeleau et al., 2019), it will be important to determine if the differential heterogeneity and plasticity of brain and spinal microglia are sex related.

Limitations of study

The data presented were generated by using the mixed gender animals. The potential sex-related differences of microglial heterogeneity could not be revealed in this study. In the future, it will be important to determine if the differential heterogeneity and plasticity of brain and spinal microglia are sex-related.

Resource availability

Lead contact

Further information and requests for resources and reagents should be directed to and will be fulfilled by the lead contact, Shao-Jun Tang (shtang@UTMB.EDU).

Material availability

This study did not generate any new unique reagents.

Data and code availability

The accession number for the data reported in this paper is GEO: GSE155081. The code used for the analysis described in this paper can be accessed at https://github.com/tang-lab/sc-microglia-heterogeneity.

METHODS

All methods can be found in the accompanying Transparent Methods supplemental file.

SUPPLEMENTAL INFORMATION

Supplemental information can be found online at https://doi.org/10.1016/j.isci.2021.102186.

ACKNOWLEDGMENTS

We thank members of the Tang laboratories for helpful discussions and comments. This study was supported by the National Institutes of Health R01 DA036165 (S.-J.T.), R01 NS079166 (S.-J.T.), and R01 NS095747 (S.-J.T.).

AUTHOR CONTRIBUTIONS

Conceptualization, S.T., J.Z., and W.R.; Methodology, J.Z., W.R., S.P., and A.P.; Investigation, J.Z., W.R., X.L., S.P., A.P., and S.Y.; Data Curation, J.A., J.Z., and M.S.; Software, J.A. and M.S.; Formal Analysis, J.Z., J.A., M.S., N.V., R.L., J.D., K.C., and R.C.; Writing – Original Draft, J.Z. and S.T.; Writing – Review & Editing, S.T. and J.Z.; Funding Acquisition, S.T.; Supervision, S.T.

DECLARATION OF INTERESTS

No disclosures were reported.

Received: August 13, 2020
Revised: December 31, 2020
Accepted: February 9, 2021
Published: March 19, 2021

REFERENCES

Aloisi, F. (2001). Immune function of microglia. Glia *36*, 165–179.

Baruch, K., Deczkowska, A., David, E., Castellano, J.M., Miller, O., Kertser, A., Berkutzki, T., Barnett-Itzhaki, Z., Bezalel, D., Wyss-Coray, T., et al. (2014). Aging-induced type I interferon response at the choroid plexus negatively affects brain function. Science *346*, 89–93.

Bialas, A.R., Presumey, J., Das, A., Van Der Poel, C.E., Lapchak, P.H., Mesin, L., Victora, G., Tsokos, G.C., Mawrin, C., Herbst, R., et al. (2017). Microglia-dependent synapse loss in type i interferon-mediated lupus. Nature *546*, 539–543.

Bordeleau, M., Carrier, M., Luheshi, G.N., and Tremblay, M.È. (2019). Microglia along sex lines: from brain colonization, maturation and function, to implication in neurodevelopmental disorders. Semin. Cell Dev. Biol. *94*, 152–163.

Bouchard, C., Pagé, J., Bédard, A., Tremblay, P., and Vallières, L. (2007). G protein-coupled receptor 84, a microglia-associated protein expressed in neuroinflammatory conditions. Glia *55*, 790–800.

Brewer, G.J., and Torricelli, J.R. (2007). Isolation and culture of adult neurons and neurospheres. Nat. Protoc. *2*, 1490–1498.

Brioschi, S., Peng, V., and Colonna, M. (2019). Fifty shades of microglia. Trends Neurosci. *42*, 440–443.

Bruce, K.D., Gorkhali, S., Given, K., Coates, A.M., Boyle, K.E., Macklin, W.B., and Eckel, R.H. (2018). Lipoprotein lipase is a feature of alternatively-activated microglia and may facilitate lipid uptake in the CNS during demyelination. Front. Mol. Neurosci. *11*, 57.

Capuccini, B., Lin, J., Talavera-López, C., Khan, S.M., Sodenkamp, J., Spaccapelo, R., and Langhorne, J. (2016). Transcriptomic profiling of microglia reveals signatures of cell activation and immune response, during experimental cerebral malaria. Sci. Rep. *6*, 39258.

Freeley, S., Kemper, C., and Le Friec, G. (2016). The "ins and outs" of complement-driven immune responses. Immunol. Rev. *274*, 16–32.

Friedman, B.A., Srinivasan, K., Ayalon, G., Meilandt, W.J., Lin, H., Huntley, M.A., Cao, Y., Lee, S.H., Haddick, P.C.G., Ngu, H., et al. (2018). Diverse brain myeloid expression profiles reveal distinct microglial activation states and aspects of Alzheimer's disease not evident in mouse models. Cell Rep *22*, 832–847.

Gehrmann, J., Matsumoto, Y., and Kreutzberg, G.W. (1995). Microglia: intrinsic immuneffector cell of the brain. Brain Res. Rev. *20*, 269–287.

Ginhoux, F., Schultze, J.L., Murray, P.J., Ochando, J., and Biswas, S.K. (2016). New insights into the multidimensional concept of macrophage ontogeny, activation and function. Nat. Immunol. *17*, 34–40.

Hammond, T.R., Dufort, C., Dissing-Olesen, L., Giera, S., Young, A., Wysoker, A., Walker, A.J., Gergits, F., Segel, M., Nemesh, J., et al. (2019). Single-cell RNA sequencing of microglia throughout the mouse lifespan and in the injured brain reveals complex cell-state changes. Immunity *50*, 253–271.e6.

Haynes, S.E., Hollopeter, G., Yang, G., Kurpius, D., Dailey, M.E., Gan, W.B., and Julius, D. (2006). The P2Y12 receptor regulates microglial activation by extracellular nucleotides. Nat. Neurosci. *9*, 1512–1519.

Hoshiko, M., Arnoux, I., Avignone, E., Yamamoto, N., and Audinat, E. (2012). Deficiency of the microglial receptor CX3CR1 impairs postnatal functional development of thalamocortical synapses in the barrel cortex. J. Neurosci. *32*, 15106–15111.

Hunt, T.W., Fields, T.A., Casey, P.J., and Peralta, E.G. (1996). RGS10 is a selective activator of Gα(i) GTPase activity. Nature *383*, 175–177.

Janova, H., Böttcher, C., Holtman, I.R., Regen, T., van Rossum, D., Götz, A., Ernst, A.S., Fritsche, C., Gertig, U., Saiepour, N., et al. (2016). CD14 is a key organizer of microglial responses to CNS infection and injury. Glia *64*, 635–649.

Keren-Shaul, H., Spinrad, A., Weiner, A., Matcovitch-Natan, O., Dvir-Szternfeld, R., Ulland, T.K., David, E., Baruch, K., Lara-Astaiso, D., Toth, B., et al. (2017). A unique microglia type Associated with restricting development of Alzheimer's disease. Cell *169*, 1276–1290.e17.

Lee, J.K., Chung, J., McAlpine, F.E., and Tansey, M.G. (2011). Regulator of G-protein signaling-10 negatively regulates NF-κB in microglia and neuroprotects dopaminergic neurons in hemiparkinsonian rats. J. Neurosci. *31*, 11879–11888.

Li, Q., Cheng, Z., Zhou, L., Darmanis, S., Neff, N.F., Okamoto, J., Gulati, G., Bennett, M.L., Sun, L.O., Clarke, L.E., et al. (2019). Developmental heterogeneity of microglia and brain myeloid cells revealed by deep single-cell RNA sequencing. Neuron *101*, 207–223.e10.

Liu, C.C., Gao, Y.J., Luo, H., Berta, T., Xu, Z.Z., Ji, R.R., and Tan, P.H. (2016). Interferon alpha inhibits spinal cord synaptic and nociceptive transmission via neuronal-glial interactions. Sci. Rep. *6*, 34356.

Liu, Y.U., Ying, Y., Li, Y., Eyo, U.B., Chen, T., Zheng, J., Umpierre, A.D., Zhu, J., Bosco, D.B., Dong, H., et al. (2019). Neuronal network activity controls microglial process surveillance in awake mice via norepinephrine signaling. Nat. Neurosci. *22*, 1771–1781.

Ma, J., Tanaka, K.F., Shimizu, T., Bernard, C.C.A., Kakita, A., Takahashi, H., Pfeiffer, S.E., and Ikenaka, K. (2011). Microglial cystatin F expression is a sensitive indicator for ongoing demyelination with concurrent remyelination. J. Neurosci. Res. *89*, 639–649.

Macosko, E.Z., Basu, A., Satija, R., Nemesh, J., Shekhar, K., Goldman, M., Tirosh, I., Bialas, A.R., Kamitaki, N., Martersteck, E.M., et al. (2015). Highly parallel genome-wide expression profiling of individual cells using nanoliter droplets. Cell *161*, 1202–1214.

Masuda, T., Sankowski, R., Staszewski, O., Böttcher, C., Amann, L., Sagar, Scheiwe, C., Nessler, S., Kunz, P., van Loo, G., et al. (2019). Spatial and temporal heterogeneity of mouse and human microglia at single-cell resolution. Nature *566*, 388–392.

Mathys, H., Adaikkan, C., Gao, F., Young, J.Z., Manet, E., Hemberg, M., De Jager, P.L., Ransohoff, R.M., Regev, A., and Tsai, L.H. (2017). Temporal tracking of microglia activation in neurodegeneration at single-cell resolution. Cell Rep. *21*, 366–380.

McMahon, S.B., and Monroe, J.G. (1996). The role of early growth response gene 1 (egr-1) in regulation of the immune response. J. Leukoc. Biol. *60*, 159–166.

Nimmerjahn, A., Kirchhoff, F., and Helmchen, F. (2005). Resting microglial cells are highly dynamic surveillants of brain parenchyma in vivo. Neuroforum *11*, 95–96.

Nomura, K., Vilalta, A., Allendorf, D.H., Hornik, T.C., and Brown, G.C. (2017). Activated microglia desialylate and phagocytose cells via neuraminidase, galectin-3, and mer tyrosine kinase. J. Immunol. *198*, 4792–4801.

Ransohoff, R.M. (2016). A polarizing question: do M1 and M2 microglia exist. Nat. Neurosci. *26*, 987–991.

Reichert, F., and Rotshenker, S. (2019). Galectin-3 (MAC-2) controls microglia phenotype whether amoeboid and phagocytic or branched and non-phagocytic by regulating the cytoskeleton. Front. Cell. Neurosci. *13*, 90.

Rothwell, N.J., and Luheshi, G.N. (2000). Interleukin 1 in the brain: biology, pathology and therapeutic target. Trends Neurosci. *23*, 618–625.

Ru, W., Liu, X., Bae, C., Shi, Y., Walikonis, R., Mo Chung, J., and Tang, S.J. (2019). Microglia mediate HIV-1 gp120-induced synaptic degeneration in spinal pain neural circuits. J. Neurosci. *39*, 8408–8421.

Schafer, D.P., Lehrman, E.K., and Stevens, B. (2013). The "quad-partite" synapse: microglia-synapse interactions in the developing and mature CNS. Glia *61*, 24–36.

Sokol, C.L., and Luster, A.D. (2015). The chemokine system in innate immunity. Cold Spring Harb. Perspect. Biol. *7*, 1–20.

Toggas, S.M., Masliah, E., Rockenstein, E.M., Rall, G.F., Abraham, C.R., and Mucke, L. (1994). Central nervous system damage produced by expression of the HIV-1 coat protein gpl20 in transgenic mice. Nature *367*, 188–193.

Wlodarczyk, A., Holtman, I.R., Krueger, M., Yogev, N., Bruttger, J., Khorooshi, R., Benmamar-Badel, A., Boer-Bergsma, J.J., Martin, N.A., Karram, K., et al. (2017). A novel microglial subset plays a key role in myelinogenesis in developing brain. EMBO J. *36*, 3292–3308.

Xuan, F.-L., Chithanathan, K., Lilleväli, K., Yuan, X., and Tian, L. (2019). Differences of microglia in the brain and the spinal cord. Front. Cell. Neurosci. *13*, 504.

Yuan, S.B., Shi, Y., Chen, J., Zhou, X., Li, G., Gelman, B.B., Lisinicchia, J.G., Carlton, S.M., Ferguson, M.R., Tan, A., et al. (2014). Gp120 in the pathogenesis of human immunodeficiency virus-associated pain. Ann. Neurol. *75*, 837–850.

iScience, Volume *24*

Supplemental information

Single-cell RNA-seq analysis reveals compartment-specific heterogeneity and plasticity of microglia

Junying Zheng, Wenjuan Ru, Jay R. Adolacion, Michael S. Spurgat, Xin Liu, Subo Yuan, Rommel X. Liang, Jianli Dong, Andrew S. Potter, S Steven Potter, Ken Chen, Rui Chen, Navin Varadarajan, and Shao-Jun Tang

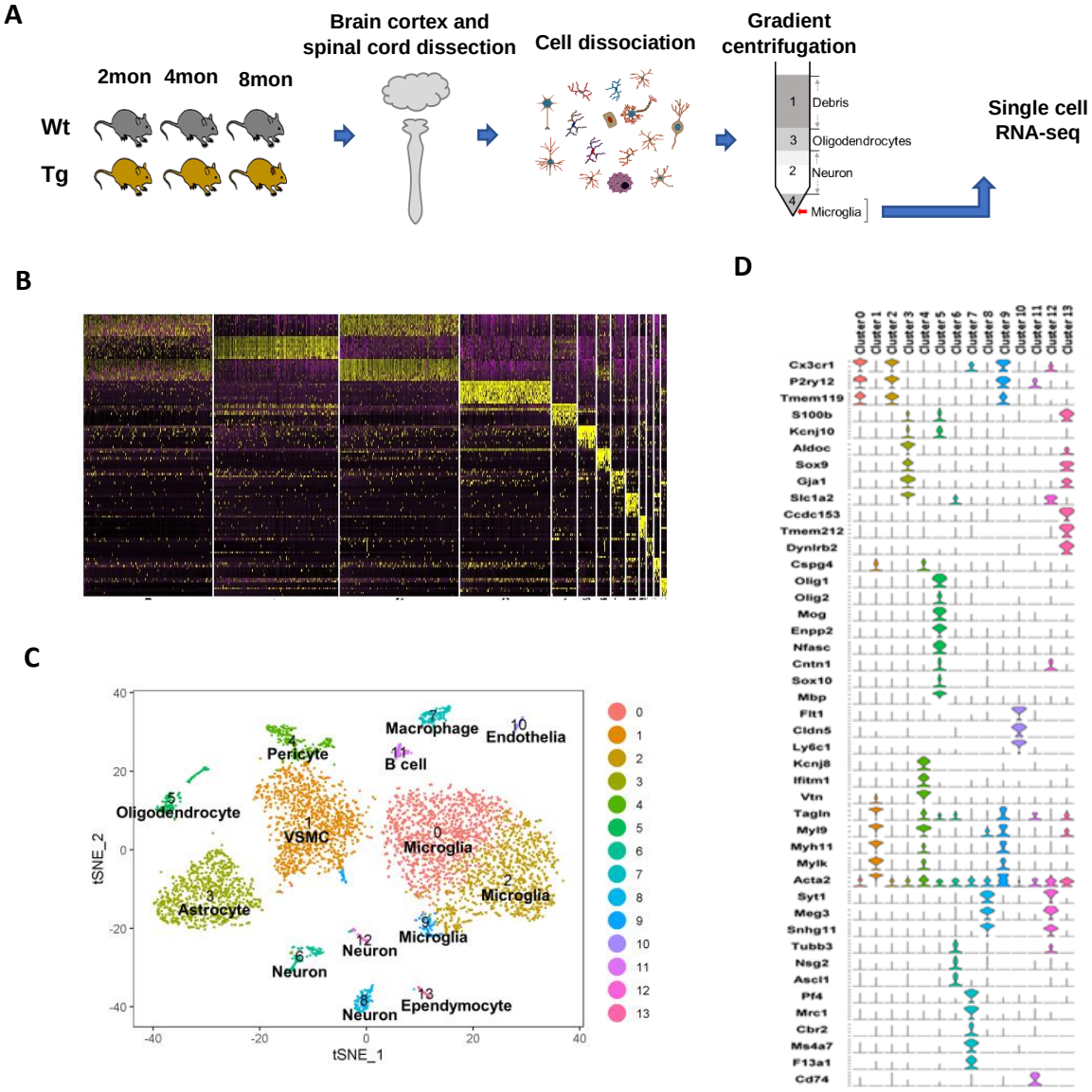

Figure S1. Workflow of the single cell RNA-seq (scRNA-seq) experiment and data analysis of cortical and spinal microglia of Wt and gp120 transgenic (Tg) mice (Related to Figure 1). A: A diagram showing the workflow of cell dissociation and scRNA-seq**.** Microglia-enriched fraction 4 was processed for the scRNA-seq. **B**. Expression heatmaps of the top 10 variable genes in each cluster demonstrated a well separated cluster. **C**. t-SNE plots displaying different cell types identified. VSMC: vascular smooth muscle cell. **D**: Combined violin plots of cell type-specific gene markers for individual clusters.

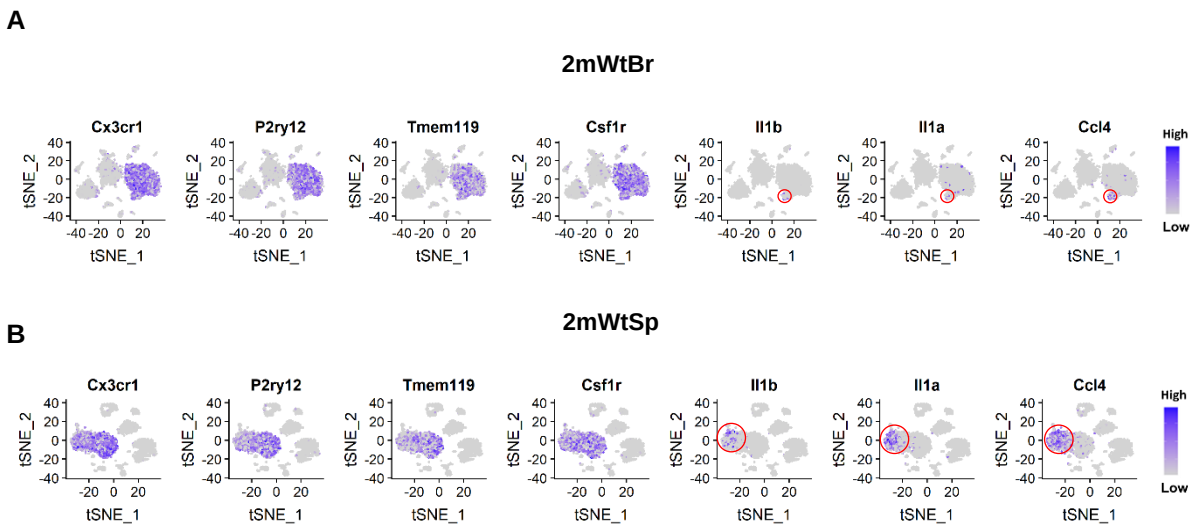

Figure S2. Feature plots of microglial marker genes and inflammatory genes showing marked differences of IFLAM-M population sizes in the cortex (2mWtBr) and the spinal cord (2mWtSp) of Wt mice at two-month-old (Related to Figure 1). Feature plots of pan-microglial marker genes Cx3cr1, P2ry12, Tmem119 and Csf1r identifying the microglial populations in the t-SNE plots of cortical (A) and spinal (B) cells. Feature plots of IFLAM-M signature genes (Il1a, Il1b, Ccl4) showing the population of IFLAM-M (red circled) in the cortex (A) and spinal cord (B). Blue: high expression. Gray: low expression.

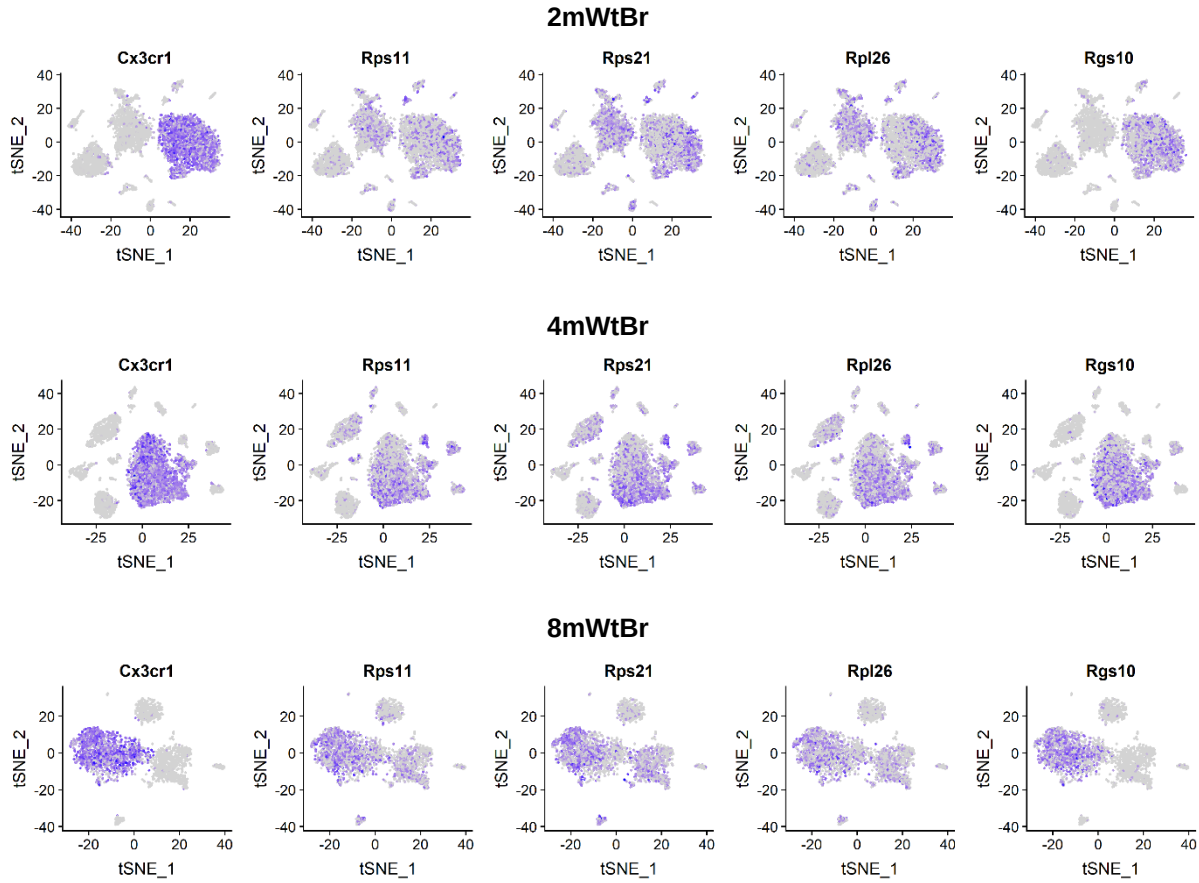

Figure S3. Feature plots showing the slightly lower expression of genes coding ribosomal proteins (e.g. Rps11, Rps21, Rpl26) and Rgs10, the gene coding a member of regulator of G protein signalling family17 in HOM-M2 microglia from the two-, four-, and eight-month-old Wt brain cortex (Related to Figure 2). The plot of Cx3cr1 shows the whole microglial clusters in each dataset.

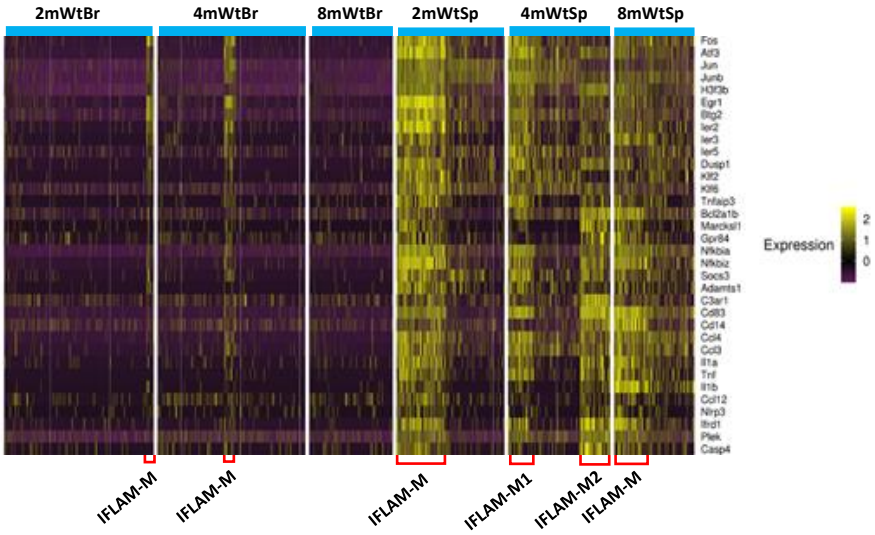

Figure S4. Gene expression heatmaps showing the IFLAM-M populations (red brackets) in the cortices and spinal cords of Wt mice at two-, four- and eight-month-old (Related to Figure 2).

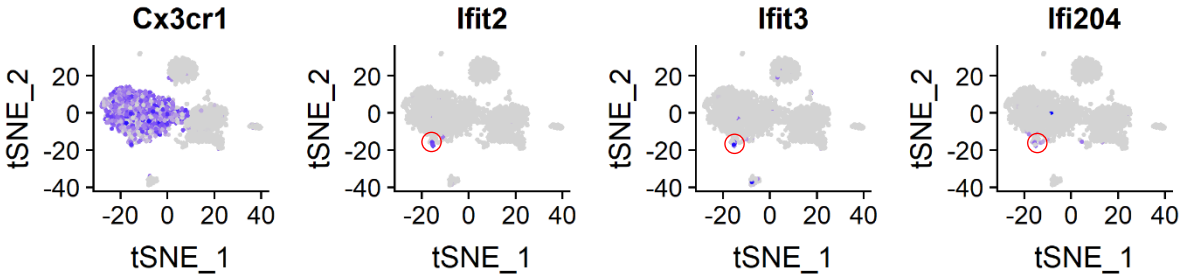

Figure S5. Feature plots show a small cortical microglial cluster with the signature of interferon-response genes (e.g. Ifit2, Ifit3, and Ifi204) in the eight-month-old Wt brain cortex (**Related to Figure 2).** The plot of Cx3cr1 demonstrates the whole microglial clusters.

Transparent Methods

Methods

Animals

Gp120 Tg mice (from Dr. Marcus Kaul, Sanford-Burnham Medical Research Institute) express HIV-1 LAV gp120 under the control of the glial fibrillary acidic protein (GFAP) promoter(Toggas et al., 1994). All animal procedures were performed according to protocol 0904031B approved by the Institutional Animal Care and Use Committee at the University of Texas Medical Branch, and all methods were performed in accordance with the relevant guidelines and regulations.

Cell dissociation from the brain cortices and spinal cords

We used the same tissue dissociation procedures to prepare brain and spinal cell dissociation in parallel. To isolate cells for scRNA-seq, Wt and gp120 Tg mice were euthanized with 14% urethane followed by decapitation. The brain cortices and whole spinal cords from the Wt and Tg mice of two, four, and eight months (n=2, mixed gender) were rapidly dissected out respectively, the brain meanings were removed thoroughly and temporarily stored in 6ml cold Hibernate A/B27 (HABG) medium. HABG was prepared by adding 30 ml of Hibernate A (BrainBits, cat. no. HA), 600µl of B27 (ThermoFisher, cat. no.17504044), 88 µl of 0.5mM Glutamax (Invitrogen, cat. no. 35050-061), penicillin-streptomycin (ThermoFisher, cat. no.15070063) to final concentration of 2%, and DNase I (ThermoFisher, cat. no. AM2224) to final concentration of 80 U/ml. After completion of dissection, the cortical or spinal tissues were separately placed in 100 mm petri dishes on ice, cut into 0.5 mm pieces with a scalpel, and transferred to a 6 well culture plate containing 6ml papain digestive medium for each sample. Digestive medium was freshly prepared by dissolving 12 mg papain powder (Worthington, cat. no. LS003119) in 6 ml Hibernate A without calcium (BrainBits, cat. no. HACA) with 15 µl 0.5 mM Glutamax, and DNase I at a final concentration of 80 U/ml. The digestive medium was activated at 37 °C for 20 to 30 min. Tissues were digested in a 37°C incubator for 1 hr (agitating every 20 min), and then transferred with the digestive medium into a 15 ml Corning tube on ice, followed by addition of 6 ml cold HABG medium. The tissues were subsequently slowly triturated on ice with a 2 ml Pasteur Pipet for 10 to 15 times. Then triturated the cells 10 to 15 times using a fire-polished narrow-bored glass pipette into single cells. The digestion was ended by adding 5 ml mixed digestion ending solution to the tissue. The ending solution was prepared by mixing 9 ml hibernate medium without calcium with 1 ml reconstituted albumin-ovomucoid inhibitor solution (Worthington, cat. No. LK003182). The dissociated cell suspension was passed through a 70 µm strainer (MACS, cat. no. 130-098-462), and centrifuged at 400×g for 5 min at 4°C. After discarding the supernatant, the cell pellets were gently resuspended in 6 ml cold HABG.

Separation of cells by density gradient centrifugation

Microglia in the cell suspension were enriched according to a published procedure(Brewer and Torricelli, 2007). Briefly, we diluted and prepared 4 ml OptiPrep (Sigma, cat. no. D1556) density gradient in a 15 ml Corning tube following the published protocol(Brewer and Torricelli, 2007). A total of 6 ml cell suspension was carefully pipetted onto the top of the density gradient and centrifuged at 800×g (Beckman, Cs-16R Centrifuge) for 30 min at 22 °C (with acceleration and deceleration rates set at 0). The top layer containing cell debris was carefully aspirated. Fraction 1 was enriched with debris, and fractions 2 and 3 were enriched with oligodendrocytes and neurons respectively (Fig. S1a)(Brewer and Torricelli, 2007). The bottom fraction (~500 µl) enriched with microglia(Brewer and Torricelli, 2007) was collected, mixed with 5 ml cold HABG medium and centrifuged for 10 min at 400×g (Beckman, Cs-16R Centrifuge) at 4°C. The cell pellet was gently resuspended in 3.1 ml cold D-PBS and was processed for additional removal of myelin and cell debris with Debris Removal Solution (Miltenyi Biotec, cat. no. 130-109-398), following the manufacturer's instructions. Cells were

suspended in HABG medium. The viability was checked using trypan blue staining. Cell preps with viability >95% were shipped (overnight on ice) to Cincinnati Children's Hospital Medical Center (to Dr. Potter) for droplet-based scRNA-seq.

Droplet-based single-cell RNA-seq

The droplet-based scRNA-seq was based on a protocol from Macosko *et. al* (http://mccarrolllab.org/wp-content/uploads/2015/05/Online-Dropseq-Protocol-v.-3.1-Dec-2015.pdf). Hydrophobic-treated microfluidic devices were ordered from Nanoshift (Richmond, CA). A total of 1.5 mL of cells (120k cells/ml) were flowed through the device along with 1.5 mL barcoded beads (Chemgenes, 175k beads/ml) and droplet generation mineral oil (QX200, Bio-Rad Laboratories). Resulting emulsion was collected in a 50 ml tube at room temperature; subsequently, the emulsion was allowed to hybridize on ice for 45 min prior to droplet breakage. The excess oil was removed, and the emulsion was transferred to a 50 mL glass conical. 40 mL of cold 6X SSC was added to the emulsion, along with 1 ml perfluorooctanol with vigorous shaking to break droplets. Following droplet breakage, beads were collected from the supernatant into two 50 ml conical tubes. The tubes were spun at 1200 g for 5 min, pelleting the beads. The supernatant was subsequently removed, and the beads were transferred to a 1.5 ml low-adhesion tube. Following this, the beads were rinsed once with 6x SSC, once with 5X RT buffer, and once with 1X RT buffer. Captured mRNAs hybridized to the beads were then reverse transcribed for 30 min at room temp. followed by 1.5 hr. at 42 °C with rotation in RT mix with 2000 U Maxima H Minus Reverse Transcriptase (ThermoFisher, MA) in 200 µl total volume. Reverse transcription was followed by an exonuclease treatment for 45 min to remove unextended bead primers. The nucleic acid on the beads were then PCR amplified (four cycles at 65 °C and 12 cycles at 67 °C annealing temperature with 3000 beads per 50 µl reaction). The cDNA from the PCR reaction was purified using 0.7x volume of SPRIselect beads (Beckman Coulter, cat. no. B23318). The quantity and quality of cDNA was measured using an Agilent Bioanalyzer hsDNA chip. To generate a library, cDNA was fragmented and amplified (12 cycles) using the Nextera XT DNA Sample prep kit with three separate reactions of 600, 1200 and 1800 pg input cDNA. The libraries were pooled and purified twice using 0.7X volume of SPRIselect beads. The purified libraries were quantified using an hsDNA chip and were sequenced on the Illumina HiSeq 2500 using the sequencing parameters described in the DropSeq protocol. The libraries were run on a single lane targeting 150 million reads per library.

Computational methods

Drop-seq FASTQ files were processed using the standard pipeline (Drop-seq tools version 1.12 from McCarroll lab, http://mccarrolllab.org/wp-content/uploads/2016/03/Drop-seqAlignmentCookbookv1.2Jan2016.pdf). Generated read counts were analysed in R version 3.4.4 (R Core Team 2018) via Seurat 2.2.1 (https://CRAN.R-project.org/package=Seurat)(Butler et al., 2018) following its standard pre-processing and clustering workflow (https://satijalab.org/seurat/v3.1/pbmc3k_tutorial.html). By default, Seurat implements a global-scaling normalization method “LogNormalize” that normalizes the gene expression measurements for each cell by the total expression, multiplies this by a scale factor (10,000 by default), and log-transforms the result. We set the filter criteria of min.genes = 300, and mitochondrial gene proportion ≤ 10% as a QC control for scRNA-seq data to remove the dead and the low-quality cells. From the distribution of reads, the data was filtered to a minimum of 300 cells per gene and 30 genes per cell. This was followed by UMI and mitochondrial filtering and normalization prior to selecting all highly variable genes falling within a selected cut-off window for PCA clustering. Statistically significant PCs (p-value < 0.001) were used in cluster determination to produce heatmaps and t-SNE plots at a resolution of 0.6. Clusters were annotated based on the expression level of canonical marker genes and gene expression visualized using feature maps. Differentially expressed genes across these clusters were generated by the FindAllMarkers function (using the MAST test) of Seurat, returning only genes with adjusted p-values < 0.05. These genes were then used to search

for enriched pathways via IPA (Ingenuity Pathways Analysis, QIAGEN Inc.). Seurat violin plots that were consolidated using graphical packages in R (Bodenhofer et al., 2011; Claus and Wilke, 2019). A number of helper functions were also employed ranging from the data input, manipulation and display (Bates and Maechler, 2014; Wickham et al., 2017; Xie, 2012) to color schemes(Neuwirth, 2014).

RNAscope *in situ* hybridization (ISH) and immunofluorescent (IF) staining

Mice were anesthetized with euthanized with 14% urethane and transcardially perfused with 30 ml cold 1xPBS. The cortex and the spinal cord were collected, and fixed in freshly prepared 4% PFA for 24 h at 4°C. The tissues were then immersed in 30% sucrose in 1xPBS at 4°C until they sank to the bottom, embedded in OCT mounting medium, and stored in an air-tight container at –80°C prior to sectioning. The mounted tissue blocks were equilibrated to –20°C in a cryostat for ~1 hour prior to sectioning. 10–20 µm cryo-sections were cut, mounted onto SuperFrost® Plus slides, and stored in airtight slide boxes in Ziplock bags at –80°C until use. Probes for the gene *Cst7* (498711-C2) and *Irf7* (cat. no. 534541-C3) were purchased from Advanced Cell Diagnostics (Newark, CA). ISH procedures, including tissue pre-treatment and probe hybridization, were performed according to the protocol of RNAscope® Multiplex Fluorescent V2 Assay provided by the manufacturer (Advanced Cell Diagnostics). Immediately after the last wash of ISH, the sections were rinsed with 1xPBS (3x5 mins), followed by immunostaining of Iba1 and nuclear staining by DAPI as described (Dual ISH-IHC, Advanced Cell Diagnostics). The stained sections on glass slides were mounted with ProLong Gold Antifade Mountant (Invitrogen, cat. no. P36930) and stored overnight at 4°C before imaging (Zeiss LSM 880 confocal microscope system). Anti-Iba1 antibody (abcam, cat. ab178847) was used at 1:200 dilution. Images were viewed using Zeiss LSM 880 with Airyscan (Carl Zeiss Microscopy GmbH) and Nikon A1R MP (Nikon Instruments Inc.). The 3-D images were processed using Imaris 9.6 software (Oxford Instruments).

Canonical pathway analysis

To evaluate the effects of HIV-1 gp120 on microglial function, upregulated genes with an adjusted p-value of < 0.05 (Benjamini-Hochberg corrected) from each cluster were imported into Ingenuity Pathway Analysis (IPA) (QIAGEN Inc.). IPA's Canonical Pathways Analysis was performed to visualize the activity of individual pathways. The significance (p-value) of the association between the dataset and the specific canonical pathway was computed using the Fisher's exact test (https://chhe.research.ncsu.edu/wordpress/wp-content/uploads/2015/10/IPA-Data-Analysis-training-slides-2016_04.pdf) with Benjamin-Hochberg multiple testing correction at $p < 0.05$ as the threshold of significance. The activation z-score was used to identify the biological pathway that were activated or inactivated. An absolute z-score of ≥ 2 was considered significant, with z-score ≥ 2 for activated pathways and a z-score≤ -2 for inactivated pathways.